DETECTION AND CHARACTERIZATION OF ACTIN MONOMERS, OLIGOMERS, AND FILAMENTS IN SOLUTION BY MEASUREMENT OF FLUORESCENCE PHOTOBLEACHING RECOVERY

FREDERICK LANNI AND B. R. WARE
Department of Chemistry, Syracuse University, Syracuse, New York 13210

ABSTRACT Fluorescence photobleaching recovery (FPR) was measured to determine the diffusion coefficient of fluorescein-labeled G-actin in low-salt buffer. The result obtained, $7.15 \pm 0.35 \times 10^{-7}$ cm^2/s, is in good agreement with that computed from the molecular weight, partial specific volume, and sedimentation coefficient, but is higher than previously obtained values. It is demonstrated from theory that at low ionic strength, the electrostatic contribution to the intrinsic viscosity leads to an overestimate of the hydrodynamic eccentricity of G-actin. Data from FPR, sedimentation, and fluorescence polarization experiments all indicate that the true low-salt form of the actin monomer has an axial ratio ≤ 3.0. The G-F transformation of actin was also observed by measurement of FPR during the assembly phase, in the steady state, and in the presence of ligands such as cytochalasin and aldolase. Each FPR record in general yields three data: relative proportion of rapidly and slowly diffusing actin, diffusion coefficient for the high-mobility fraction, and a mean diffusion coefficient for the low-mobility fraction. A relation between the mean low-mobility diffusion coefficient and the number-average filament length is derived and applied to the analysis of FPR data. Under typical conditions, the average filament length was $>>10$ μm in the steady state. Cytochalasin D was found to decrease filament length and total amount of filament proportionally; total filament number was not greatly affected. In all polymerizations of G-actin, the high-mobility material observed in situ was found to be essentially monomeric actin. Relatively stable oligomers of actin were separated by fractionating G-AF-actin by gel filtration in 50 μM $MgCl_2$ at 4°C. On the basis of the diffusion coefficient, we conclude that monomer and dimer constitute the major particle types present under these conditions. Sedimentation of labeled actin polymerized in 1.0 mM $MgCl_2$ yielded a graded supernatant that contained actin oligomers significantly larger than the monomer.

INTRODUCTION

The cytoskeletal and contractile system of motile cells must have the versatility to perform any of several active functions. Correspondingly, the cytoplasm of single cells shows much less spatial structure than is found in muscle tissue, and this structure is often transient or periodic in time as well. In characterizing cytoplasm, or reconstituted solutions of its components, the translational and rotational mobilities of the macromolecules provide unambiguous measures of dynamic constraints. The technique of fluorescence photobleaching recovery (FPR; Peters et al., 1974; Axelrod et al., 1976; Edidin et al., 1976; Jacobson et al. 1976; and Koppel et al., 1976) permits measurement of the translational mobility, usually expressed as the diffusion coefficient, D_T, of labeled macromolecules in solution and in domains having cellular or subcellular dimensions. When coupled with the methodology of fluorescent analogue cytochemistry (FAC; Taylor and Wang, 1978), FPR provides a means to observe and quantify cytoplasmic molecular dynamics with high selectivity and sensitivity in vivo.

Two aspects of FPR measurement make it a method of choice for the study of complex macromolecular mixtures. First, because it is a tracer measurement, the fluorescence signal always corresponds to a single component in the mixture, whereas the viscosity or light-scattering cross section represents the integrated effect of all components. Second, the measurement of FPR does not mechanically stress the specimen. In highly entangled, gelled, or cross-linked systems, the application of stress can cause irreversible changes in structure to occur.

The in vitro experimental results reported here are part of an effort to understand the G-F transformation of actin, the central protein of cytoplasmic motility, in terms that allow interpretation of the results of in vivo experiments (Wojcieszyn et al., 1981; Kreis et al., 1982; and Wang et al., 1982). In an earlier paper (Lanni et al., 1981), we

Reprint requests should be addressed to Dr. Ware.

Dr. Lanni's present address is the Center for Fluorescence Research in Biomedical Sciences, Carnegie-Mellon University, Pittsburgh, PA.

reported a basic observation regarding the polymerization of actin as reflected in the FPR record; the fluorescence recovery of polymerizing or steady state actin is split into two well-defined mobility ranges, one of which is characteristic of the free diffusion of a globular protein, and the other representing the slow diffusion of long filaments. This observation is essential for verification of the phase-condensation model (Oosawa and Kasai, 1971) and the more recent head-to-tail model (Wegner, 1976) of actin polymerization. Here we extend the above observations and address the question of the nature of the high-mobility particles present in steady state with F-actin under a variety of conditions.

EXPERIMENTAL PROCEDURES

Materials

Actin was prepared from rabbit muscle acetone powder (Pel-Freez Inc., Rogers, AK) by the procedure of Spudich and Watt (1971). The purity of the actin was tested by SDS polyacrylamide gel electrophoresis (procedure of Laemmli and Favre, 1973); on heavily overloaded gels, low-molecular-weight proteins could be detected to constitute 5% or less of the total protein. Cytochalasins and aldolase were obtained from Sigma Chemical Co., St. Louis, MO.

Labeled Actin

AF-actin was prepared by reacting F-actin with 5-iodoacetamido-fluorescein (5-IAF; Molecular Probes, Inc., Junction City, OR) by a modification of the procedure of Wang and Taylor (1980). For all polymerization experiments, labeled actin was mixed with unlabeled actin in the ratio 1:3 (at the most) down to 1:15 (6% AF-actin). Dilution of labeled actin with native actin was important to prevent fluorescence quenching by neighboring fluorescein residues in the filament. Also, we previously reported a photochemical artifact associated with photobleaching F-actin in which a large fraction of the subunits carry fluorescent labels.

Solutions

Native actin and AF-actin were stored as hydrated pellets of F-actin on ice and in the dark. Thymol crystals or 0.02% sodium azide were used to retard microbial growth. Actin to be used in experiments was resuspended at a concentration of 1–5 mg/ml in 1–2 ml buffer A (Tris 2.0 mM, Na_2 ATP 0.2 mM, $CaCl_2$ 0.2 mM, 2-mercaptoethanol 0.5 mM, pH 8.0, 25°C; Spudich and Watt, 1971) and dialyzed in 140 ml of the same buffer at 4°C for a minimum of 12 h. During this period, the dialysis buffer was replaced at least once to ensure depletion of Mg^{+2} from the protein. Preservatives were not added to dialysis buffers, since 0.02% NaN_3 increases the ionic strength of buffer A from ~3 to 6 mM. To maintain actin in the monomeric (G) state, it was desirable to keep the buffer ionic strength as low as possible. Furthermore, it was noted that thymol, azide, and also ascorbate and thiols suppressed the photobleaching reaction of fluorescein to varying degrees. The remarkable protective action of another phenol, *n*-propyl gallate, against photobleaching of fluorescein and rhodamine has also recently been reported (Giloh and Sedat, 1982).

Dialyzed solutions of G-actin were clarified by centrifugation at 10^5 *g* for 30 min at 4°C. The supernatants were transferred to clean polystyrene or polycarbonate tubes and stored on ice in the dark. Under these conditions, G-actin stock solutions were stable for at least 3 d, and showed no loss of polymerizability over this period.

FPR Specimens

FPR specimens were prepared by mixing labeled G-actin, native G-actin, buffer, and other components, and immediately loading 5 μl of the solution into washed flat glass microcapillary tubes having a depth of 100 μm (Vitro Dynamics, Rockaway, NJ). The capillary was placed on a flat black, anodized aluminum plate, and each end was sealed with a drop of coverslip mounting cement (Permount, Fisher Scientific Co., Pittsburgh, PA). Convection or lateral flow were never detected in this type of specimen.

FPR specimens of G-actin in low-salt buffer were stable for many hours. After prolonged incubation at room temperature (>12 h) fluorescence recoveries showed that a small amount (<5%) of the actin became immobile due to either polymer formation or adhesion to the walls of the glass capillary tube. The effect of the container on the results obtained in these experiments was never significant.

When salt (KCl), $MgCl_2$, or other ligands were added to G-actin in buffer, it was desirable to obtain the first FPR record as quickly as possible so as to observe the early stages of the G-F transformation. Time zero ($t = 0$) in all experiments was defined by the addition of other components to the G-actin solution. It was possible to have a completely assembled one-specimen slide in position on the FPR instrument within 120 s. For each specimen, FPR measurements were made at separate locations along the capillary. This reduced the local radiation dose received by the specimen, and avoided interference from the slowly dissipating pattern components of the previous measurement.

FPR Measurement

FPR data were recorded using the modulation detector instrument described by Lanni and Ware (1982). For a single, freely diffusing molecular species, the form of the fluorescence recovery will be

$$E(t)/E(0) = e^{-Dk^2t} \tag{1}$$

where $E(t)$ is the residual modulation of a periodic pattern of spacing P bleached into the specimen at $t = 0$, $k = 2\pi/P$, and D is the translational tracer diffusion coefficient of the molecular species. If a fraction of the labeled component is not free to diffuse, then part of the bleached pattern in the specimen will persist, and the recovery follows the function

$$E(t)/E(0) = (1 - f)e^{-Dk^2t} + f \tag{2}$$

where f is the immobile fraction. In these experiments the filamentous actin constitutes a slowly diffusing, but not truly immobile fraction (in the absence of cross links). The fluorescence recovery of this low-mobility fraction is not mono-exponential, due to the great heterogeneity of the F-actin in terms of filament length. As long as the actin filaments diffuse freely, the complete expression for the fluorescence recovery can be written as

$$E(t)/E(0) = f_{HM}e^{-D_{HM}k^2t} + f_{LM}\sum_n a(n)e^{-D(n)k^2t} \tag{3}$$

where f_{LM} is the low-mobility fraction ($f_{HM} + f_{LM} = 1$), $D(n)$ is the diffusion coefficient for an n subunit polymer, $a(n)$ is the normalized weight concentration of such polymer, and D_{HM} is the diffusion coefficient of the high-mobility fraction. It can be shown that the weight-average diffusion coefficient of the filaments is then given by the ratio of the initial recovery rate of the LM fraction to the initial amplitude of the LM fraction:

$$\langle D_{LM}\rangle = -E'_{LM}(0)/k^2E_{LM}(0)$$

$$= \sum_n nc(n)D(n) \Big/ \sum_n nc(n) \tag{4}$$

where $c(n)$ is the molar concentration of n subunit polymer. Therefore, three independent parameters can be derived from actin FPR data; D_{HM}, the high mobility diffusion coefficient, f_{LM}, the low-mobility fraction, and $\langle D_{LM}\rangle$, the mean low-mobility diffusion coefficient.

In practice, Eq. 2 or Eq. 5 (Results) was fit to an FPR data record by direct minimization of the mean-square error. In many cases, a ruler and

pencil sufficed to obtain $E'_{LM}(0)$ and $E_{LM}(0)$ directly from chart records because of the large difference in rate of diffusion of the high- and low-mobility components.

Sedimentation Experiments

KCl (up to 50 mM) or $MgCl_2$ (up to 1.0 mM) was added to G-AF-actin in low-salt buffer. After 1 h incubation at 25°C, a 1-cm hydrostatic column of each solution was centrifuged at 10^5 *g* at 15°C. FPR specimens were prepared from each supernatant.

Gel-Filtration Experiments

AF-actin was depolymerized and dialyzed in low-salt buffer containing no Ca^{+2}, but with 50 μM $MgCl_2$. Sedimentation at 10^5 *g* for 30 min at 4°C produced no pellet, establishing by the usual criterion that the actin was G-actin. This actin was then passed through a 110-cm column of Sephadex G-150-120 equilibrated with the same buffer at 4°C. The peak fluorescent fractions were used in the preparation of FPR specimens.

Ligand Experiments

Cytochalasins D and B (Sigma Chemical Co.) were used as model ligands. Stock solutions of each toxin were made in 95% ethanol. All control solutions of actin had an equal amount of ethanol (1.2% maximum) added. FPR specimens were prepared immediately after mixing, and the rate and final state of the G-F transformation monitored by sequential FPR measurement. The best results were obtained when a test specimen and a control specimen were mixed at the same time, mounted together on the FPR instrument, and tested alternately. With this procedure, the incubation time, loading, and temperature history were as similar as possible for each specimen and its control.

Aldolase, a glycolytic protein known to bind reversibly to F-actin, was used as a model macromolecular ligand. Unlabeled aldolase (Sigma Chemical Co.) was dialyzed in low-salt buffer and added to the actin solution just before the addition of polymerization buffer. FPR specimens were prepared as outlined above. An earlier attempt to use fluorescein-labeled aldolase, prepared by reacting the enzyme with fluorescein isothiocyanate in the presence of saturating substrate, resulted in an active, fluorescent enzyme which had lost all affinity for F-actin.

RESULTS

Diffusion Coefficient of G-AF-Actin

FPR specimens of G-AF-actin in low-salt buffer yielded data records that could be fit with a single exponential term and no significant low-mobility fraction (Fig. 1). Actin concentrations of 1.6, 0.8, and 0.4 mg/ml were used, with no significant difference in the measured time constants. With a pattern period of 118 μm (k = 533 cm^{-1}) the data were best fit by a time constant of 0.205 (±0.010 SE) s^{-1}. From this value, measured at 20.4°C, the diffusion coefficient corrected to 20.0°C is (7.15 ± 0.35) × 10^{-7} cm^2/s for G-(AF)-actin in buffer A. As a test to determine that only diffusive motion was contributing to the fluorescence recovery, a second set of measurements was made with a pattern period of 74.7 μm (k = 841 cm^{-1}). These data yielded a time constant of 0.503 (±0.019 SE) s^{-1}. This gives a temperature-corrected diffusion coefficient of (7.03 ± 0.26) × 10^{-7} cm^2/s, in good agreement with the value obtained for k = 533 cm^{-1}. We consider the value measured with the coarser pattern to be less affected by systematic error, since the fluorescence recoveries were slower and more accurately recorded.

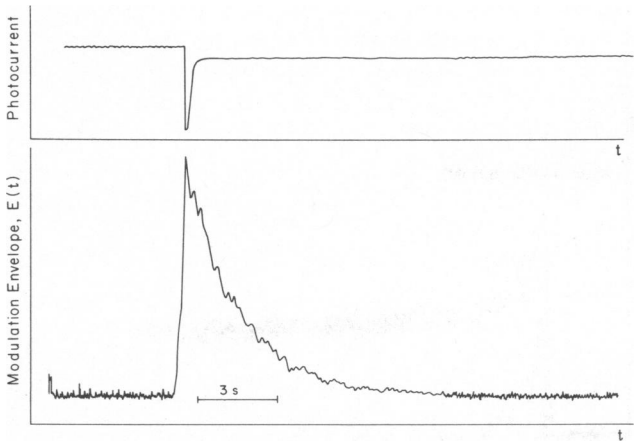

FIGURE 1 Fluorescence photobleaching recovery of G-AF-Actin in low salt buffer. AF-actin was depolymerized by dialysis in buffer A at 4°C and clarified by centrifugation at $10^5 g$ for 30 min. The supernatant was used to prepare a 5 μl FPR specimen having an actin concentration of 0.8 mg/ml. The temperature of the specimen was maintained at 20.4°C in the FPR instrument. The *upper* trace shows the DC component of the photocurrent which is a measure of total fluorescence emission (λ > 515 nm) before and after bleaching. The current is constant during the recovery phase of the measurement because essentially only a redistribution of fluorescence occurs. The *lower* trace shows the decay of the modulation (contrast) of the periodic pattern bleached into the solution. The modulation envelope [$E(t)$] decays exponentially with a time constant equal to $1/Dk^2$ where D is the diffusion coefficient and $k = 2\pi$ /(periodic pattern spacing). For the above record, $k = 2\pi$ /(74.7 μm) = 841 cm^{-1}, and the measured time constant was equal to 1.97 s; therefore, the diffusion coefficient, corrected to 20.0°C, equals 7.10 × 10^{-7} cm^2/s.

Polymerization of Actin

The effects of adding salt (KCl) to a solution of G-actin are typified by the FPR data presented in Fig. 2. Initially, complete dissipation of the photo-bleached pattern was observed (f_{LM} = 0), and a diffusion coefficient between 7 × 10^{-7} cm^2/s and 8 × 10^{-7} cm^2/s was computed from the measured time constant. In subsequent FPR records, an increasing fraction of the fluorescence modulation was persistent, as indicated in Fig. 2 by the difference between the prebleach modulation level and the level of the limiting part of each record ($t \geqq 10$ s). The FPR records obtained clearly show a high-mobility fraction that is distinct from the low-mobility fraction. Each record was analyzed in terms of Eq. 2; the high-mobility diffusion coefficient (D_{HM}) was computed from the decay time constant, and the low-mobility fraction (f_{LM}) was determined. In each case, D_{HM} was in the range 7–8 × 10^{-7} cm^2/s, which is very close to the actin monomer diffusion coefficient. The relative invariance of D_{HM} through the G-F transformation is shown in Fig. 3 for two different concentrations of KCl.

The graph of the low-mobility fraction over time (Fig. 4) shows that there was initially a period in which little or no low-mobility actin formed (see also Fig. 10 and 11) followed by a period in which actin was maximally converted from the high-mobility form to a low-mobility form

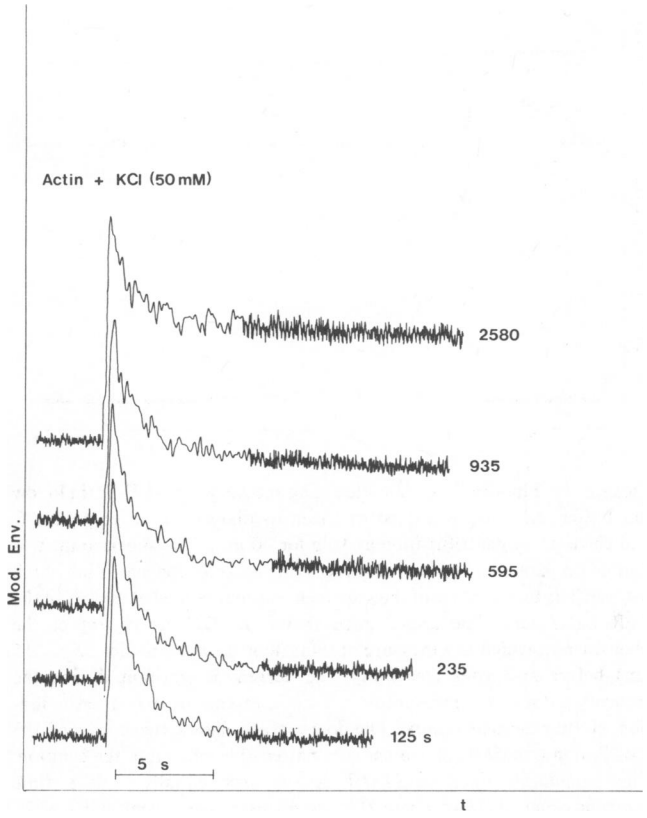

FIGURE 2 FPR records for polymerization of 0.75 mg/ml actin in 50 mM KCl. 100 mM KCl in 40 μl buffer A were added to 40 μl of G-actin (native + AF = 1.5 mg/ml) at $t = 0$ (Mod. Env., modulation envelope). An FPR specimen was quickly prepared and measurements were made at intervals of several minutes. Initially, the fluorescence recovery shows that only rapidly diffusing actin is present in the solution, but subsequent records show that an increasing fraction of the photobleached pattern persists due to the formation of polymeric actin that diffuses much more slowly. Each measurement was recorded first at a high chart speed, then six times slower to compress the data record. The elapsed time (in seconds) is indicated to the *right* of each record. For this specimen, a periodic pattern of spacing 74.7 μm was used ($k = 841$ cm^{-1}).

(F-actin). The steady state level of f_{LM} was sensitive to the solution composition; an increased concentration of KCl in the specimen caused faster conversion of actin to the F-form and established a higher steady state level in less time.

The slow phase of the fluorescence recovery was never observed to be mono-exponential, thus reflecting the heterogeneous nature of the F-actin in terms of filament length. Two procedures were used to obtain the mean diffusion coefficient of the low-mobility actin during the G-F transformation. Slowly polymerizing specimens yielded FPR records which were accurately described by a linearized version of Eq. 3:

$$E(t)/E(0) = f_{HM}e^{-D_{HM}k^2t} + f_{LM}(1 - \langle D_{LM}\rangle k^2t). \quad (5)$$

In rapidly polymerizing specimens and in specimens approaching the steady state, the F-actin mobility was generally too low to detect with the coarse photobleaching

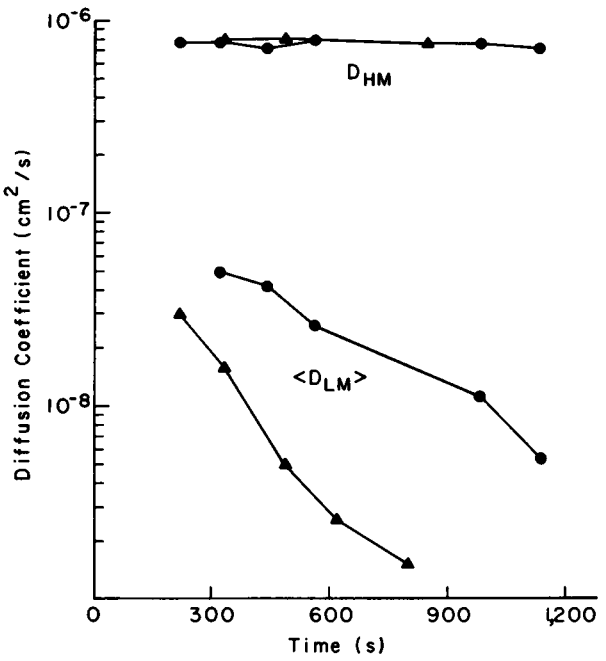

FIGURE 3 Diffusion coefficients of the HM and LM fractions as a function of time during actin polymerization in 50 and 17 mM KCl. D_{HM} was computed from the decay time constant of the HM fraction from each record in a series similar to those of Fig. 2. $\langle D_{LM}\rangle$ was computed from the linear decay rate and amplitude of the LM fraction or from a second FPR record made with a finer periodic pattern. The HM diffusion coefficient was essentially stationary through the G-F transformation. The average LM diffusion coefficient decreased monotonically with time from 3–5 × 10^{-8} cm^2/s for the earliest data records to <2 × 10^{-9} cm^2/s after 600 s (50 mM KCl). The concentration of actin in these specimens was 4.8 mg/ml. (▲, 50 mM KCl) and 6.4 mg/ml (●, 17 mM KCl).

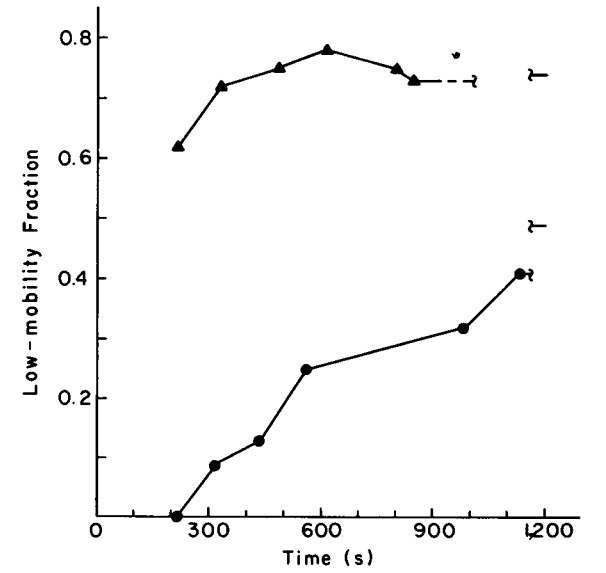

FIGURE 4 Low-mobility fraction as a function of time during actin polymerization in 50 and 17 mM KCl. f_{LM} was measured in a series of records similar to those of Fig. 2. The standard error is ~0.05 units. (▲) 50 mM KCl; (●) 17 mM KCl.

pattern (period = 118 or 74.7 μm), requiring a second measurement to be made with a finer pattern (period = 29.5 μm). The computed values of $\langle D_{LM} \rangle$ are presented in Fig. 3 for two different concentrations of KCl. In contrast to the parameter D_{HM}, the mean F-actin mobility was found to decrease strongly with time.

When millimolar $MgCl_2$ was substituted for monovalent salt in these experiments, much more rapid conversion of actin to the polymeric form was observed. The rapid appearance of F-actin after addition of $MgCl_2$ to a solution of G-actin (0.5–2.5 mg/ml) made it impossible with our current equipment to measure FPR in the early stages of the G-F transformation; a significant low-mobility fraction was always present in the first record of the sequence. The rapid change of state that occurred in the solution also limited the acceptable duration of each FPR record; our data analysis is based on the premise that the filament length distribution is changing slowly relative to the duration of each record. The limiting value of f_{LM} attained by Mg-polymerized specimens was typically so close to 1.0 that the diffusion coefficient of the high-mobility fraction could not be accurately computed for the steady state. However, the FPR records made early in each sequence do show well-defined, high-mobility and low-mobility fractions. The high-mobility diffusion coefficient computed from such data is close to the actin-monomer coefficient. From the FPR data in Fig. 5, recorded 275 s after addition of $MgCl_2$ to 1.0 mM to G-actin at a concentration of 0.5 mg/ml, the computed value of the diffusion coefficient was 7.1×10^{-7} cm^2/s, which is not measurably different from that found for G-actin in low-salt buffer. D_{HM} was again found to be nearly constant during the polymerization, while $\langle D_{LM} \rangle$ decreased strongly with time (Fig. 6). The steady state values of the low-mobility fraction that were attained with 1.0–2.5 mM $MgCl_2$ are well above the levels obtained under similar conditions with 50–100 mM KCl (Fig. 7).

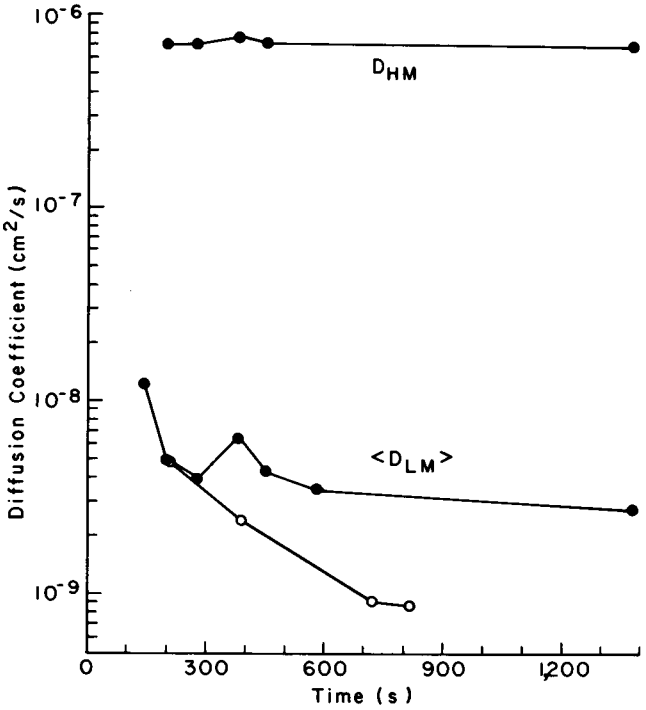

FIGURE 6 Diffusion coefficients of the HM and LM fractions as a function of time during actin polymerization in 1.0 and 2.5 mM $MgCl_2$. As in the salt-induced G-F transformation (Fig. 3), D_{HM} remained stationary while $\langle D_{LM} \rangle$ decreased strongly with time. The concentration of actin in these specimens was 0.5 mg/ml (●, 1.0 mM $MgCl_2$) and 0.4 mg/ml (○; 2.5 mM $MgCl_2$).

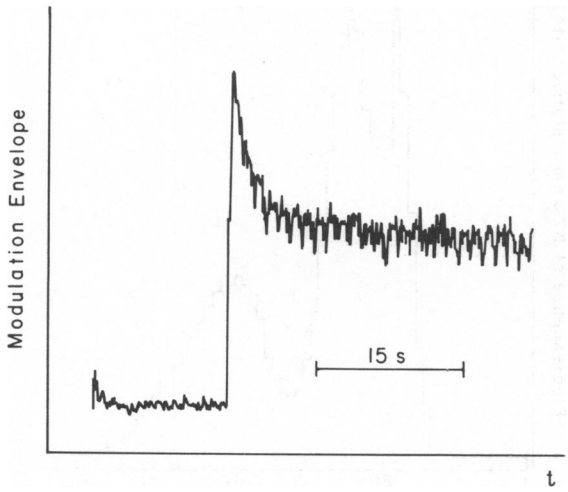

FIGURE 5 Fluorescence photobleaching recovery record of actin in 1.0 mM $MgCl_2$. At $t = 0$, $MgCl_2$ was added to a solution of G-actin (10% AF) so that the final concentrations were 1.0 mM (Mg) and 0.5 mg/ml (actin). The above record was made 275 s after the addition. The low-mobility fraction at this point was equal to 0.49, but eventually exceeded 0.75.

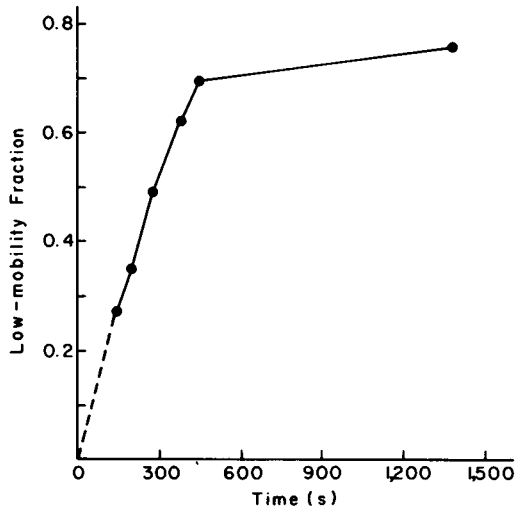

FIGURE 7 Low-mobility fraction as a function of time during actin polymerization in 1.0 mM $MgCl_2$. f_{LM} was measured from the same series of records as presented in Figs. 5 and 6; actin concentration = 0.5 mg/ml. Under these conditions, the early stages of the polymerization process were complete before the first measurement could be made, so the existence of a "lag phase" could not be tested.

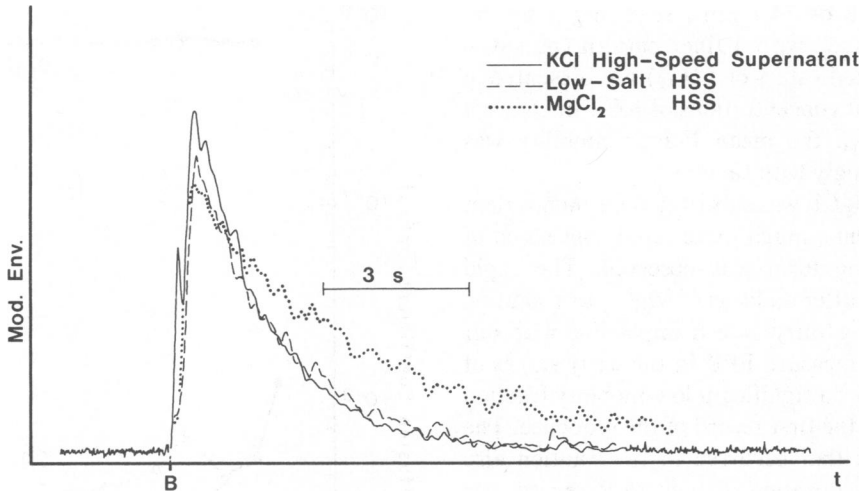

FIGURE 8 FPR records for sedimentation experiment. G-actin, or solutions of actin polymerized with 50 mM KCl or 1.0 mM $MgCl_2$ were sedimented in an ultracentrifuge to remove F-actin (see text). FPR specimens were prepared from each high-speed supernatant (HSS). Particles diffusing more slowly than actin monomer were the major species in the Mg-HSS, but did not form distinct HM and LM fractions (*Mod. Env.*, modulation envelope).

The result of sedimenting polymerized actin solutions is shown by the FPR data of Fig. 8. The undisturbed 50 mM KCl supernatant and the control supernatant were homogeneously pale yellow by transmitted light. The diffusion coefficients computed from FPR data records were between 7×10^{-7} cm^2/s and 8×10^{-7} cm^2/s indicating that the supernatant actin in these specimens was essentially monomeric. In contrast, the undisturbed 1.0 mM $MgCl_2$ supernatant had a graded appearance in transmitted light, being colorless at the meniscus and pale yellow above the pellet. The supernatant was sampled slightly lower than midway between meniscus and pellet. The diffusion coefficient computed from the FPR data record in this case was 4×10^{-7} cm^2/s, approximately half that of the actin in the other supernatants. After several hours of incubation at room temperature, the KCl and $MgCl_2$ supernatants did slowly form more polymer, as detected by a nonzero low-mobility fraction. This may have been a result of the hydrostatic pressure on the actin and the lower specimen temperature during centrifugation.

Gel-filtration of G-AF-actin through G-150-120 Sephadex equilibrated with 50 μM $MgCl_2$, as described in Experimental Procedures, resulted in a trimodal distribution of fluorescence among the fractions as shown in Fig. 9. Total running time for the column was ~15 h; therefore, interconversion among the different-sized actin species present must be a very slow process at 4°C. FPR specimens of the peak fractions 18, 24, and 39 were tested at 20°C (Table I). The diffusion coefficient of the smallest particles to elute from the column (fraction No. 39) was 6.9×10^{-7} cm^2/s, close to that of the actin monomer. The next larger particles (fraction No. 24) yielded a coefficient of 4.9×10^{-7} cm^2/s. The fluorescent leading fractions traveled slightly behind the void volume of the column and, when tested at 20°C, gave a diffusion coefficient of 2.6×10^{-7} cm^2/s. However, the actin in the FPR specimen prepared from fraction #18 formed a low-mobility component at 20°C, and it is therefore unlikely that the measured diffusion coefficient corresponds to a homogeneous species of actin in the solution. All three of the peak fractions polymerized rapidly and to a high degree upon addition of millimolar $MgCl_2$ to each.

The kinetic effects of cytochalasin *B* (CB) and cytochalasin *D* (CD) on the G-F transformation of actin are shown in Figs. 10 and 11, respectively. We observed that both

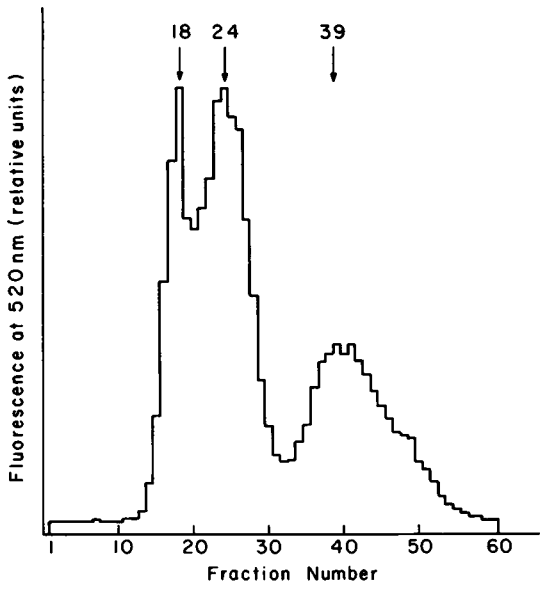

FIGURE 9 Gel-filtration experiment. AF-actin was depolymerized in buffered 50 μM $MgCl_2$, and clarified by sedimentation. The supernatant was applied to a 110-cm column of Sephadex G-150-120 equilibrated with the same buffer at 4°C. The fluorescence of each fraction was measured at 4°C with an excitation wavelength of 490 nm.

TABLE I
FPR HIGH-MOBILITY-FRACTION ACTIN DIFFUSION COEFFICIENTS*

Preparation	$D \times 10^7$ cm^2/s (20°C)
Low-salt buffer¶ (G-AF-actin)	7.15 ± 0.35
100 mM KCl polymerization	7.25 ± 0.27‡
1.0 mM $MgCl_2$ polymerization	7.18 ± 0.33§
50 mM KCl supernatant	7.5 ± 0.5
1.0 mM $MgCl_2$ supernatant	4.0 ± 0.5
50 μM $MgCl_2$ G-150 fractions prepared at 4°C	
No. 39 (trailing)	6.9
No. 24 (middle)	4.9
No. 18 (leading)	2.6‖

*Tracer fluoresceinthiocarbamyl-Cys(374) actin.
‡KCl concentrations in the range 17 mM to 100 mM gave essentially this result.
§The very small HM fractions in near-steady-state specimens exhibited slightly slower diffusion.
‖Specimen not likely to be homogeneous with respect to particle size.
¶Low-salt buffer (buffer A) contains 0.2 mM Ca^{+2}.

toxins increased the rate of formation of polymeric actin in 50 mM KCl solution. In addition, cytochalasin D acted to shorten the duration of the period before which a detectable quantity of polymer formed. CD, and to a lesser extent CB, reduced the amount of F-actin in the steady state solutions relative to control specimens that contained only trace ethanol (solvent used for cytochalasin). These observations are in accord with the results of the fluorescence enhancement experiments of Tellam and Frieden (1982) and the FPR experiments of Tait and Frieden (1982).

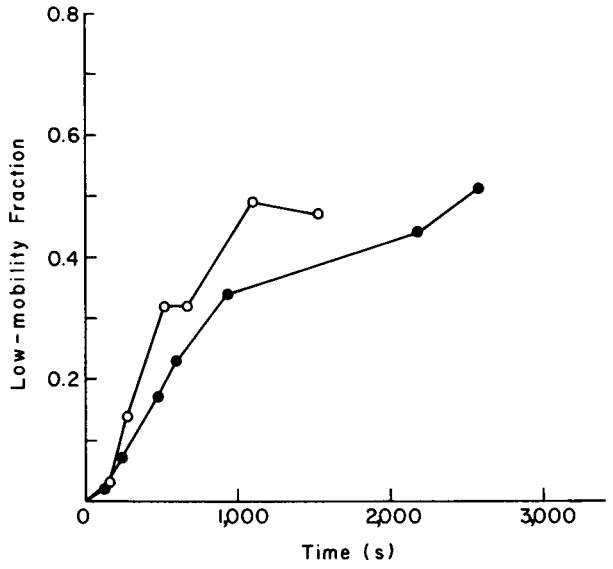

FIGURE 10 Effect of cytochalasin B on the low-mobility fraction during actin polymerization in 50 mM KCl. Cytochalasin B in a small volume of ethanol was added to G-actin in low-salt buffer. A control solution received only ethanol. Buffered KCl was then added to both and FPR specimens prepared (o, CB; •, control). The final concentration of actin in the specimens was 0.75 mg/ml (18 μM), and the test specimen contained a total concentration of 6 μM CB.

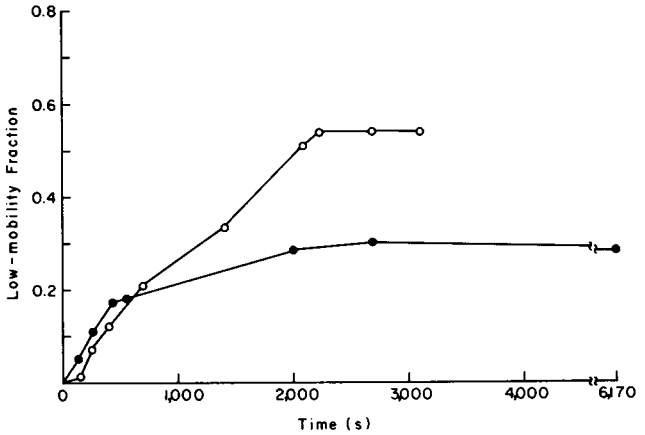

FIGURE 11 Effect of cytochalasin D on actin LM-fraction during polymerization in 50 mM KCl. Using the same procedure as outlined for CB, a dual specimen (o, control; •, 25μM total CD) was prepared and FPR measured during the G-F transformation. CD increased the initial rate of formation of F-actin and decreased the steady state LM-fraction relative to the control.

Observation of the diffusion of G-actin and F-actin in control and cytochalasin-treated specimens was accomplished by use of a coarse photobleaching pattern (k = 841 cm^{-1}) and a fine pattern (k = 2127 cm^{-1}) obtainable by switching from a 6.3X to a 16X objective lens for each pair of records. The FPR records presented in Fig. 12 show fluorescence recovery in both high- and low-mobility fractions in a 0.75 mg/ml solution of actin 20 h after addition of KCl to 50 mM. By use of Eq. 3, we computed the mean diffusion coefficient of the low-mobility fraction; in the control specimen $\langle D_{LM} \rangle = 7.7 \times 10^{-10}$ cm^2/s, and in the 25 μM CD specimen, $\langle D_{LM} \rangle = 1.44 \times 10^{-9}$ cm^2/s. A similar effect was also observed with cytochalasin B. In pure actin solutions (in the absence of cross-link–forming ligands), we did not observe the extreme immobilization of filaments reported by Tait and Frieden (1982). We attribute this difference to our use of 50 mM KCl, which causes less vigorous polymerization than the 2.0 mM $MgCl_2$ used in their experiments.

In cytochalasin-treated actin specimens that had incubated for many hours, a reduced mobility was obtained for the high-mobility fraction. This can be seen by comparing the two upper traces of Fig. 12. The relaxation time constant for the 25 μM CD specimen is approximately double that of the control specimen; therefore, particles larger than the actin monomer were present. This effect was not observed in the early stages of the G-F transformation where the high-mobility fraction is essentially G-actin, and did not occur in the control specimen which had trace ethanol but no cytochalasin.

The monotonic relationship between steady state F-actin content (f_{LM}) and total CD content is shown in Fig. 13 for a 0.75 mg/ml (18 μM) solution of actin 20 h after addition of KCl to 50 mM. At a total concentration of 6 μM, cytochalasin D reduces f_{LM} by 15% relative to the control

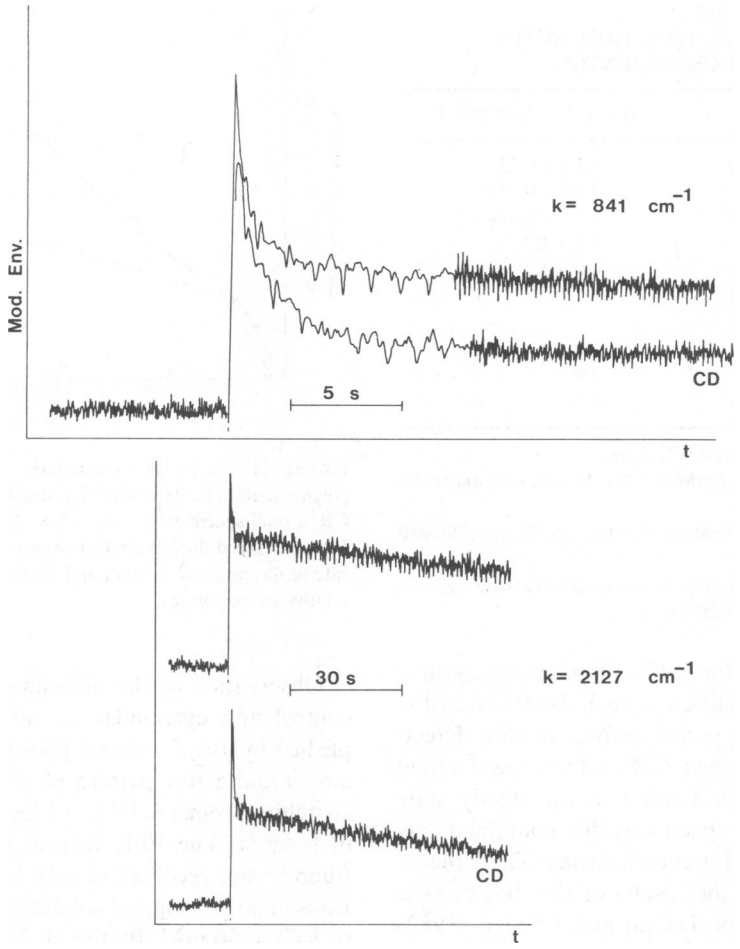

FIGURE 12 FPR records showing effect of cytochalasin D on actin polymerization (Mod. Env., modulation envelope). FPR measurements were made on solutions of actin polymerized in 50 mM KCl (20 h at 25°C). The test specimen contained a total concentration of 25 μM CD, and both contained actin at 0.75 mg/ml. $D_{HM\%E \text{ and } f_{LM}}$ were obtained from measurements made with a coarse pattern (k = 841 cm^{-1}). To get $\langle D_{LM} \rangle$ accurately, each specimen was also tested with a fine pattern (k = 2,127 cm^{-1}).

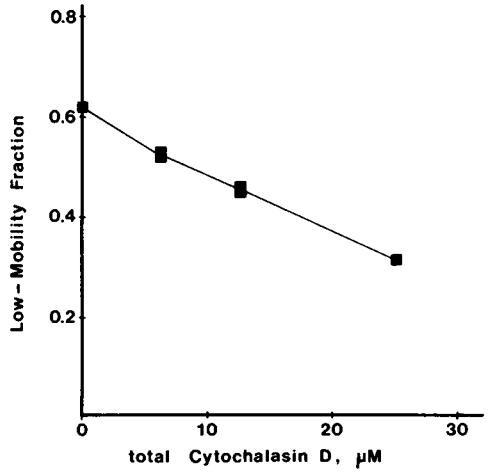

FIGURE 13 Effect of cytochalasin D on the steady state LM fraction in 50 mM KCl. From a series of specimens of 18 μM actin polymerized in the presence of 0, 6.2, 12.5, and 25 μM CD, the steady state value of f_{LM} as a function of total CD was measured. The concentration of free CD was not determined.

specimen; the same amount of cytochalasin B caused a 10% reduction in f_{LM}. Because the reduction of f_{LM} is nearly linear with added cytochalasin D, Fig. 13 suggests that close to 50 μM CD, no F-actin will form in 50 mM KCl; alternatively, less strongly polymerizing conditions could be found that would reduce f_{LM} to zero in the CD range used here. It would be interesting to determine what type of aggregates form under these conditions. These results corroborate the effects of CD on the actin critical concentration reported by Tellam and Frieden (1982).

Highly immobile filamentous actin was produced when actin was allowed to polymerize in the presence of rabbit muscle aldolase. FPR records of steady state specimens with and without the added enzyme show that more actin polymer is formed in the presence of aldolase and that this polymer diffuses much more slowly (if at all) than the F-actin in the control specimen. This result is in accord with the known multivalent actin-binding properties of the enzyme under similar solution conditions (Arnold and Pette, 1968; Clarke and Morton, 1976).

DISCUSSION

Diffusion Coefficient of G-Actin

Previous estimates of the diffusion coefficient of G-actin have been made from sedimentation boundary measurements (Mihashi, 1964) and from FPR measurements (Lanni et al., 1981). The higher value, 6.1×10^{-7} cm^2/s, computed from FPR data is still significantly lower than the value reported here. We attribute this difference to systematic error resulting from the FPR measurement procedure in use at that time. The exponential data generated by the FPR modulation detector is strongly convergent in an analytic sense, and the computed time constant is insensitive to the exact choice of the zero time point in the data record. For these reasons, systematic error is a lesser problem in our new results.

The value of the diffusion coefficient obtained for G-AF-(ATP)-actin is in good agreement with the theoretical value calculated using the sedimentation coefficient (S), molecular weight (M), and partial specific volume (υ). The elementary relation $S = M(1 - \rho\upsilon)/Nf$ gives the hydrodynamic frictional coefficient of the molecule. The factor $M(1 - \rho\upsilon)$ is invariant with isopycnic hydration so that the polypeptide molecular weight and partial specific volume can be used here as a good approximation to the hydrodynamic values. The Einstein relation $D_T = kT/f$ expresses the translational tracer diffusion coefficient in terms of the frictional coefficient. Using the values $S_{20,w} = 3.25 \times 10^{-13}$ s (Lewis et al., 1963), $\upsilon = 0.750$ ml/gm (Rees and Young, 1967), and $M = 42{,}000$ (Elzinga et al., 1973), $D_T = 7.54 \times 10^{-7}$ cm^2/s at 20°C in water, which is close to the value computed from our data, 7.15×10^{-7} cm^2/s. The "anhydrous" volume of the protein can be calculated from the molecular weight and partial specific volume: $V_A = M\upsilon/N = 5.2 \times 10^4$ Å^3.

The hydrodynamic volume of G-actin includes at least the volume of hydrating water. If it is assumed that roughly 0.3 g water hydrates each gram of protein, the total volume (V) is increased to 7.3×10^4 Å^3. The minimum frictional coefficient occurs for a spherical monomer of radius $R_s = (3V/4\pi)^{1/3}$; the ratio f/f_{min} is a measure of the departure of the shape of the molecule from being spherical and compact. From the above numbers, this ratio has the value 1.15, which corresponds to a prolate ellipsoid of approximate axial ratio 3.5. The same computation performed with the value of D_T calculated from M, υ, and S yields $f/f_{min} = 1.10$, or an axial ratio of 3.0. These values are considerably less extreme than early estimates of the axial ratio or total hydrodynamic volume of G-actin (Mihashi, 1964; Lewis et al., 1963).

Electron microscopy of F-actin or of two-dimensional crystals of Gd^{+3}-actin (Aebi et al., 1980) shows that the axial ratio of actin monomers in these structures is closer to 2 than to 3. Because measurements made upon solutions of G-actin are necessarily made at low ionic strength to suppress assembly of filaments, there are two effects to consider in explaining the difference between the axial ratio computed from hydrodynamic data and that taken from electron microscope images. The first possibility is that electrostatic forces between ionized residues on the protein cause it to expand or change shape in low-salt buffer so that the hydrodynamic dimensions actually increase. The effect would be a reduction of the diffusion coefficient that would be independent of protein concentration. A particle of axial ratio 2.0 would diffuse as if it were an equi-volume particle of axial ratio 3.5 if its total hydrodynamic volume were increased by a factor of 34% at constant axial ratio. It is difficult to imagine that large structural changes occur however, because actin rapidly denatures upon loss of bound nucleotide (Straub and Feuer, 1950) and because none of the five cysteine residues of the protein form intramolecular disulfide bonds. These facts indicate that limited flexibility of the structure may be critical.

The second possibility is that the electrostatic charge of the protein molecule affects bulk and tracer hydrodynamic properties through the interaction of macro ion and counter ions or between macro ions. These interactions would not depend upon expansion of the protein at low ionic strength. Early estimates of the expanded volume or axial ratio of G-actin in solution both relied upon measurement of the intrinsic viscosity ($[\eta]$) of G-actin; this value was found to be 0.10 dl/g for both G-ADP-actin (Mihashi, 1964) and G-ATP-actin (Lewis et al., 1963) and is significantly higher than for other globular proteins of comparable molecular weight (typically 0.03–0.04 dl/gm, Tanford, 1961). The connection between the intrinsic viscosity and molecular shape is made by the Einstein-Simha equation $\eta = \eta_o(1 + \phi\nu)$ or $[\eta] = \upsilon\nu$ where $\phi = c\upsilon$ is the volume fraction occupied by the dissolved particles at concentration c, and ν is Simha's coefficient which equals 5/2 for spherical particles and otherwise is related to the axial ratio of the particles by a tabulated function.

The intrinsic viscosity is sensitive to not only hydrodynamic size and shape, but also to the electrostatic interaction between macro ions and counter ions. The electroviscous effect studied by Bull (1940) and analyzed by Booth (1950) is the bulk manifestation of the distortion of the equilibrium distribution of counter ions around a macro ion due to hydrodynamic shear. An equation was derived by Booth that relates the "excess" viscosity of a solution to the macro ion charge and the mobility and ionic strength of the counter ions. The magnitude of the electroviscous effect is generally small, but any quantity that is a function of the specific viscosity (such as $[\eta]$) can be significantly affected. Written in terms of the intrinsic viscosity, Booth's result for spherical macro ions of charge z and radius a is

$$[\eta] = [\eta]_{ES} + [\eta]_{el} = (5/2)\bar{v}\left[1 + q^*\left(\frac{ze^2}{\epsilon akT}\right)^2 Z(\kappa a)\right]$$

where $[\eta]_{ES}$ is the intrinsic viscosity that would be measured in the absence of charge (or at high ionic strength) given by the Einstein-Simha equation, and $[\eta]_{el}$ is the electroviscous contribution. q^* is a valence-squared-weighted average of the counter ion frictional coefficients, and $Z(\kappa a)$ is a dimensionless function of the product of the macro ion radius and the Debye-Huckel screening constant (κ) which is an increasing function of ionic strength.

The conductivity of buffer A at room temperature is $0.44 \times 10^{-3}\Omega^{-1}\text{cm}^{-1}$, roughly equivalent to a 3 mM solution of KCl. The value of the inverse Debye-Huckel screening constant is therefore ~55 Å, slightly less than twice the mean radius of the actin subunits observed in F-actin by electron microscopy. An approximation of $[\eta]_{el}$ can be made by assuming the electrostatic charge on the protein to be $-14e$, $(\kappa a) = 0.5$, and the electrolyte to be 3 mM KCl; under these circumstances $[\eta]_{el} = 2.7\ [\eta]_{ES}$; i.e., the electroviscous contribution to the total intrinsic viscosity is almost three times as large as the electroneutral term. As an example, this factor would cause spherical macro ions to appear to have an axial ratio of ~7–8 as a result of their charge. This indicates that the measured value of the intrinsic viscosity for G-actin cannot be used directly in the computation of hydrodynamic parameters. An approximate correction to the intrinsic viscosity $[\eta]' = [\eta]/(1 + 2.7)$ therefore equals 0.03, similar to values observed for other globular proteins.

Comparison of Tracer and Mutual Diffusion Measurements

In the FPR experiments outlined here, the translocation of labeled particles acted upon by random forces was measured over a pattern of known dimensions. Macroscopic concentration gradients were nonexistent in the solutions used, so that any one diffusing particle moved in an isotropic average environment. The observed mobility is expressed by the tracer diffusion coefficient computed from FPR data.

In contrast, the technique of quasi-elastic light scattering (QELS) allows observation of the concentration fluctuations of particles in solution: the mutual diffusion coefficient is determined from QELS data. A result of QELS theory is that electrostatic interaction between macro ions will increase the measured value of the mutual diffusion coefficient significantly at low ionic strength (Berne and Pecora, 1976). The physical picture for this effect is that electrostatic repulsion between macro ions and relatively rapid counter ion diffusion decreases the lifetime of a concentration inhomogeneity. In contrast, tracer diffusion is impeded by electrostatic repulsion between macro ions, so that the mutual diffusion coefficient and the tracer diffusion coefficient should diverge at finite macro ion concentration at low ionic strength. What is not clear, however, is the effect of counter ion diffusion on the diffusion of the macro ion at infinite macro ion dilution. This is the microscopic version of the electroviscous effect. A theory for the electrostatic contribution to the frictional coefficient of a macro ion has been constructed by Schurr (1980) and indicates that tracer diffusion is slowed by macro ion charge even at infinite dilution relative to the zero-charge or high-ionic strength limits. FPR experiments provide an ideal means to test this theory.

A comparison of the tracer coefficient measured by FPR with the value obtained for G-actin by QELS (8.13×10^{-7} cm^2/s, Montague, et al., 1983) shows that the difference between the two values is in the expected direction for finite macro ion concentration and low ionic strength. The "electroneutral" diffusion coefficient of G-actin, which reflects its true physical shape in solution, should therefore fall between the tracer and mutual values. At high ionic strength, the values of the two coefficients should converge. Our data generally show higher values of D_{HM} in high-salt solutions of actin (Table I), but the precision of these values is currently too low to determine a limiting value for D_{HM}.

Measurement of steady state fluorescence polarization (Cheung et al., 1971) or pulse anisotropy decay results in a determination of the rotational relaxation time (t^R) of the labeled particles in solution. Pulse anisotropy decay measurements were made by Mihashi and Wahl (1975) of *N*-etheno-ATP bound to G-actin in low-salt buffer, with the result that $t^R = 117$ ns at 5°C. From the relation between t^R and the rotational diffusion coefficient, $t^R = 1/2D_R = 4\pi\eta a^3/kT$, the mean particle radius was computed to be $a = 28.6$ Å. The translational diffusion coefficient at 20°C should therefore be 7.49×10^{-7} cm^2/s. In another study by Ikkai et al., (1979), G-actin covalently labeled with a naphthyl probe gave a value $t^R = 135$ ns at 3.5°C in buffer A. The computed mean particle radius is 29.5 Å, and the equivalent translational diffusion coefficient at 20°C is 7.26×10^{-7} cm^2/s.

Rotational diffusion should not be as severely affected as translational diffusion by electrostatic effects between macro ions or between a macro ion and its counter ions. It can be seen from the above cited results that the computed diffusion coefficients fall between the measured tracer coefficient and the measured mutual coefficient. The preceding arguments lead to the conclusion that G-actin in solution is a hydrodynamic particle of (prolate) axial ratio certainly <3.5, and very likely <3.0.

Polymerization of Actin

High-Mobility Species. The cooperative effect by which a small aggregate of actin monomers presents a high-affinity binding site for further addition of monomer is a key idea in the phase condensation model of the G-F transformation of actin (Kasai et al., 1962*a*,*b*; Oosawa and Kasai, 1971). A result of this nucleation step is that a well-defined population of sub-nuclear aggregates (including monomer) and a population of filamentous actin should

be detectable in a polymerizing or steady state or equilibrium solution. Different methods have been used to demonstrate such a partition, usually by separating filamentous actin from the small particles by sedimentation, and quantification of pellet and supernatant protein content. The FPR data presented here show both fractions simultaneously. In accord with the phase condensation model, or the more recent head-to-tail model (Wegner, 1976), our data show that the two fractions are well-defined; i.e., there is a large mobility difference between the particles that constitute each.

It is of interest to determine the nature of the small aggregates of actin that constitute the HM fraction. In a polymerizing solution, the composition of the HM fraction is affected mainly by the incorporation of monomer into filaments. As the total number of filaments approaches a maximum, dissociation or filament-breaking processes also contribute significantly to the HM particle population (Wegner 1982; Wegner and Savko, 1982). Dissociation processes could conceivably result in the separation of small aggregates from F-actin, rather than separation of only monomers, so that the HM fraction in the steady state is not restricted to be identical in composition to the HM fraction in the early phase of the G-F transformation.

Our data show that when actin polymerization is induced by the addition of salt to buffer A (which contains 0.2 mM $CaCl_2$), the diffusion coefficient of the HM fraction is essentially that of the actin monomer (Fig. 3, Table I). Therefore, higher aggregates and filament nuclei must constitute only a small percentage of the HM particles present. In the steady state, we also observed that the HM fraction has the mobility of the actin monomer, so that dissociative processes must essentially contribute monomer back into the HM pool. This is confirmed by the results of our sedimentation experiment; the high-salt supernatant is composed of particles that diffuse as fast as the actin monomer (Fig. 8). The same result was obtained (with less precision) during the assembly phase of the $MgCl_2$-induced G-F transformation. The HM fraction diffusion coefficient is that expected for monomeric actin.

In contrast to undisturbed actin solutions, the results of our sedimentation experiment demonstrate that under certain conditions, a large population of actin oligomers can be produced that are relatively stable. The labeled particles present in the 1.0 mM $MgCl_2$ supernatant had an average mobility slightly more than 50% that of G-actin. Because the translational diffusion coefficient is a relatively weak function of the linear dimensions of the hydrodynamic particle, dimerization of actin does not suffice to explain our result. Crude models based on particle volume and equivalent hydrodynamic ellipsoids show that a compact tetramer or extended trimer are the smallest aggregates that would account for the magnitude of the observed result.

Gel filtration of dilute G-actin in the presence of 100 mM KCl demonstrates that monomeric actin is the only significant species present below the critical concentration (Pardee and Spudich, 1982). In 150 mM KCl + 0.1 mM $CaCl_2$, actin also elutes as a monomeric species at 4°C (Rouayrenc and Travers, 1981). The elution profile for actin in 50 μM $MgCl_2$ shows two distinct oligomeric species to be present. The diffusion coefficient for the smaller species shows it to be actin monomer. An approximate model of the actin dimer based upon molecular volume and shape shows that the observed diffusion coefficient of the larger species (4.9×10^{-7} cm^2/s) is close to that expected on theoretical grounds. Furthermore, at 4°C, the dimer fractions contain about as much actin as the monomer fractions. If this amount of actin dimer was present during $MgCl_2$-induced polymerization of G-actin at 20°C the HM fraction would show a reduced mobility, which is not the case. Therefore, it can be concluded that either the relative proportions of monomer and oligomer are highly temperature dependent or that the actin dimer population is produced during depolymerization of F-actin in the presence of a low concentration of magnesium ion. Both alternatives can be tested by extending the protocols used here.

The different results obtained from testing undisturbed actin solutions, from supernatants, and from gel-filtration fractions lead us to conclude that the state of an actin solution is very sensitive to its thermodynamic history in terms of temperature, pressure, and chemical potentials.

Low-Mobility Species. Graphs of the LM fraction over time after addition of salt to G-actin in buffer A show positive curvature initially (Figs. 4, 10, 11). This is the same result obtained under a variety of conditions by measurement of flow birefringence of actin solutions during the G-F transformation (Kasai et al., 1962*a*; Yin et al., 1981; Marnyama, 1981) or by measuring light scattering (Wegner, 1982), viscosity (Kasai et al., 1962*b*; Isenberg et al., 1980), or fluorescence enhancement (Tellam and Frieden, 1981). From a theoretical standpoint the curvature is a result of the cooperative processes by which weakly associating monomers form a nucleus that then presents a high-affinity site for further additions of monomer. However, measurements of ATP hydrolysis rate (Asakura and Oosawa, 1960; Mommaerts, 1952; Kasai et al., 1962*b*), measurements of OD232 (Gordon et al., 1976; Pardee and Spudich, 1982), and measurements of fluorescence resonance energy transfer (Taylor et al., 1981) do not show the initial positive curvature. As noted by Pardee and Spudich, the phenomena of flow birefringence, viscosity, and light scattering all result from processes that weight the effects of long filaments much more heavily than short filaments. The result is an exaggeration of curvature in the graphs. However, FPR measurements, as well as the fluorescence-enhancement assay, weight filament length proportionally (Eq. 3), and therefore should accurately reflect the amount of polymerized actin in the specimen at a given time. It was not possible with the data presented

here to detect initial curvature of the graph of $f_{LM}(t)$ for polymerization with $MgCl_2$.

In the absence of significant interaction between filaments, it should be possible to derive a relationship between the mean LM-fraction diffusion coefficient ($\langle D_{LM} \rangle$) and some measure of the average length of the particles that constitute the LM fraction in solutions of actin. As expressed by Eq. 4, $\langle D_{LM} \rangle$ is an average of D_{LR}, the diffusion coefficient of a long rod molecule at infinite dilution, weighted by the distribution of actin monomers into filaments of all sizes. For a condensation polymer, the length distribution in the steady state is exponential (Oosawa, 1970), so that the monomer distribution function can be written generally as $p(x) = x\, e^{-x\langle L \rangle/N}$ where $p(x)dx$ is the fraction of the total actin incorporated into polymer having a length in the range $[x, x + dx]$, N is a normalization constant, and $\langle L \rangle$ is the number-average length of the polymer. Treating F-actin approximately as a long cylinder of length x and diameter w, the translational diffusion coefficient

$$D_{LR}(x) = \frac{kT}{3\pi\eta x}[\ln(x/w) + 0.49]$$

can be derived from the orientationally-averaged frictional coefficient of a highly prolate ellipsoid. The result of averaging $D_{LR}(x)$ with the weighting $p(x)$, subject to the restriction that $\langle L \rangle >> a,w$ (where a = minimum filament length), is that $\langle D_{LR} \rangle$ is nearly equal to $D_{LR}(\langle L \rangle)$:

$$\langle D_{LM} \rangle = \frac{kT}{3\pi\eta\langle L \rangle}[\ln(\langle L \rangle/w) - 0.09] \qquad (6)$$

Therefore, the LM-fraction mean diffusion coefficient can be used to compute the number-average filament length of steady state F-actin. The above expression for $\langle D_{LM} \rangle$ does not account for the effect of interference between long filaments, or for the flexibility of individual filaments. Table II lists values of $\langle L \rangle$ and corresponding values of $\langle D_{LM} \rangle$.

In our experiments, the low-mobility fraction reached a steady level within roughly 30 min after salt or $MgCl_2$ was added to the solution of G-actin. As pointed out by Oosawa (1970), the time required for the most probable length distribution to be reached can far exceed the time required for f_{LM} to reach a plateau. Measurement of filament lengths by electron microscopy was performed by Kawamura and Maruyama (1970) with the result that Poisson-type distributions were obtained in very early stages of the G-F transformation (1–80 min, 0.1 M KCl, 0.1 mg/ml actin, 25°C) and exponential distributions from solutions approaching a true steady state. Under solution conditions where the treadmill rate of the actin is significant, the filament lengths may reach a steady state distribution in much less time (Wegner, 1976). In the data presented here, we cannot assume a steady state distribution of lengths in our FPR specimens, so for this reason, and because we do not account for interference between diffusing filaments, our use of the expression for $\langle D_{LM} \rangle$ can only approximate $\langle L \rangle$ at this point.

TABLE II
MEAN LM-FRACTION DIFFUSION COEFFICIENT AND CORRESPONDING VALUES OF THE NUMBER-AVERAGE FILAMENT LENGTH (EQ. 6)*

$\langle L \rangle$	$\langle D_{LM} \rangle$
μm	cm^2/s
0.1	1.04×10^{-7}
1.0	2.03×10^{-8}
10.0	3.02×10^{-9}
100.0	4.00×10^{-10}

*w = 80Å, T = 20°C.

In the polymerization of 2.3 mg/ml actin in 50 mM KCl (Fig. 3) the value of $\langle D_{LM} \rangle$ 600 s after initiation was 2.6×10^{-9} cm^2/s. In accord with Oosawa's model, $\langle D_{LM} \rangle$ was still a decreasing function of time even though f_{LM} had reached a stationary value of ~75%, indicating that the filament length distribution was not yet stationary. With the diameter of the hydrodynamic cylinder that models F-actin set equal to 80 Å (Moore et al., 1970), the computed average filament length is 12 μm.

A significantly lower mobility was measured during the polymerization of 0.40 mg/ml actin in 2.5 mM $MgCl_2$. 800 s after initiation, $\langle D_{LM} \rangle$ was equal to 8.7×10^{-10} cm^2/s which corresponds to filaments of average length 41 μm. The lowest mobility that we observed in solutions of pure actin was measured 20 h after polymerizing 0.75 mg/ml actin in 50 mM KCl; $\langle D_{LM} \rangle = 7.7 \times 10^{-10}$ cm^2/s. This corresponds to a mean filament length of 47 μm. In all of the above examples the computed average filament length is large relative to the average center-of-mass separation between filaments so that collisions between filaments must affect the measured values of $\langle D_{LM} \rangle$ and therefore of $\langle L \rangle$.

Comparison of $\langle D_{LM} \rangle$ determined after a long incubation with and without 25 μM cytochalasin D (Fig. 12) shows that the average filament length was reduced from 47 to 23 μm by the ligand. Because the amount of F-actin in the CD specimen was also halved relative to the control (Fig. 13), the total number of actin filaments present in the steady state was therefore not greatly affected by the ligand. As pointed out by Mozo and Ware (1984), this suggests that cytochalasin D functions by capping the fast-assembly end of actin filaments under these conditions (KCl-polymer) rather than by causing random fragmentation of filaments.

Because an FPR experiment is a set of tracer measurements that do not mechanically perturb the specimen, they afford a unique means to study structure and dynamics in fragile or weakly ordered systems. As demonstrated here,

information about size and size distribution is available from FPR data. Measurement of translational mobility by FPR, and rotational mobility by fluorescence polarization, should serve well to characterize the structure and dynamics of cytoplasm or other complicated macromolecular substances. In the domain of chemical physics, FPR measurements allow exploration of the electrostatic contribution to the hydrodynamic friction of macro ions in solution.

The technical assistance of Mrs. Mara Aistars is gratefully acknowledged.

This work was supported by grant No. PCM-8010924 from the National Science Foundation.

Received for publication 1 August 1983 and in final form 22 February 1984.

REFERENCES

Aebi, U., P. R. Smith, G. Isenberg, and T. D. Pollard. 1980. Structure of Crystalline Actin Sheets. *Nature (Lond.).* 288:296–298.

Arnold, H., and D. Pette. 1968. Binding of glycolytic enzymes to structure proteins of the muscle. *Eur. J. Biochem.* 6:163–171.

Asakura, S., and F. Oosawa. 1960. Dephosphorylation of adenosine triphosphate in actin solutions at low concentrations of magnesium. *Arch. Bioch. Biophys.* 87:273–280.

Axelrod, D., D. E. Koppel, J. Schlessinger, E. Elson, and W. W. Webb. 1976. Mobility measurement by analysis of fluorescence photobleaching recovery kinetics. *Biophys. J.* 16:1005–1069.

Berne, B. J., and R. Pecora. 1976. Dynamic Light Scattering. J. Wiley & Sons, Inc., New York.

Booth, F. 1950. The electroviscous effect for suspensions of solid spherical particles. *Proc. R. Soc. Lond. A. Math. Phys. Sci.* 203:533–551.

Bull, H. B. 1940. The electroviscous effect in egg albumin solutions. *Faraday Soc. Trans.* 36:80–84.

Cheung, H. C., R. Cooke, and Lynne Smith. 1971. The G-actin → F-actin transformation as studied by the fluorescence of bound dansyl cystine. *Arch. Biochem. Biophys.* 142:333–339.

Clarke, F. M., and D. J. Morton. 1976. Aldolase binding to actin-containing filaments. *Biochem. J.* 159:797–798.

Edidin, M., Y. Zagyansky, and T. J. Lardner. 1976. Measurement of membrane protein lateral diffusion in single cells. *Science (Wash. DC).* 191:466–468.

Elzinga, M., J. H. Collins, W. M. Kuehl, and R. S. Adelstein. 1973. Complete amino-acid sequence of actin of rabbit skeletal muscle. *Proc. Natl. Acad. Sci. USA.* 70:2687–2691.

Giloh, H., and J. W. Sedat. 1982. Fluorescence microscopy: reduced photobleaching of rhodamine and fluorescein protein conjugates by *n*-propyl-gallate. *Science (Wash. DC).* 217:1252–1255.

Gordon, D. J., Y.-Z. Yang, and E. D. Korn. 1976. Polymerization of acanthamoeba actin. *J. Biol. Chem.* 251:7474–7479.

Ikkai, T., P. Wahl, and J.-C. Auchet. 1979. Anisotropy decay of labelled actin. *Eur. J. Biochem.* 93:397–408.

Isenberg, G., U. Aebi, and T. D. Pollard. 1980. An actin-binding protein from *acanthamoeba* regulates actin filament polymerization and interactions. *Nature (Lond.).* 288:455–459.

Jacobson, K., E. Wu, and G. Poste. 1976. Measurement of the translational mobility of concanavalin A in glycerol-saline solutions, and on the cell surface by fluorescence recovery after photobleaching. *Biochim. Biophys. Acta.* 433:215–222.

Kasai, M., S. Asakura, and F. Oosawa. 1962*a*. The G-F equilibrium in actin solutions under various conditions. *Biochim. Biophys. Acta.* 57:13–21.

Kasai, M., S. Asakura, and F. Oosawa. 1962*b*. The cooperative nature of G-F transformation of actin. *Biochim. Biophys. Acta.* 57:22–31.

Kawamura, M., and K. Maruyama. 1970. Electron microscopic particle length of F-actin polymerized in vitro. *J. Biochem.* 67:437–457.

Koppel, D., D. Axelrod, J. Schlessinger, E. Elson, and W. W. Webb. 1976. Dynamics of fluorescence marker concentration as a probe of mobility. *Biophys. J.* 16:1315–1329.

Kreis, T. E., B. Geiger, and J. Schlessinger. 1982. Mobility of microinjected rhodamine actin within living chicken gizzard cells determined by fluorescence photobleaching recovery. *Cell.* 29:835–845.

Laemmli, U. K., and M. Favre. 1973. Maturation of the head of bacteriophage T4. *J. Mol. Biol.* 80:575–599.

Lanni, F., D. L. Taylor, and B. R. Ware. 1981. Fluorescence photobleaching recovery in solutions of labeled actin. *Biophys. J.* 35:351–364.

Lanni, F., and B. R. Ware. 1982. Modulation detection of fluorescence photobleaching recovery. *Rev. Sci. Instrum.* 53:905–908.

Lewis, M. S., K. Maruyama, W. R. Carroll, D. R. Kominz, and K. Laki. 1963. Physical properties and polymerization reactions of native and inactivated G-actin. *Biochemistry.* 2:34–39.

Maruyama, K. 1981. Effects of trace amounts of Ca^{+2} and Mg^{+2} on the polymerization of actin. *Biochim. Biophys. Acta.* 667:139–142.

Mihashi, K. 1964. Molecular characteristics of G-ADP-actin. *Arch. Biochem. Biophys.* 107:441–448.

Mihashi, K., and P. Wahl. 1975. Nanosecond pulsefluorometry in polarized light of G-actin-ε-ATP and F-actin-ε-ADP. *FEBS (Fed. Eur. Biochem. Soc.) Lett.* 52:8–12.

Mommaerts, W. F. H. M. 1952. The molecular transformations of actin, III. *J. Biol. Chem.* 198:469–475.

Montague, C., K. W. Rhee, and F. D. Carlson. 1983. Measurement of the translational diffusion constant of G-actin by photon correlation spectroscopy. *J. Muscle Res. Cell Motil.* 4:95–101.

Moore, P. B., H. E. Huxley and D. J. DeRosier. 1970. Three-dimensional reconstruction of F-actin, thin filaments and decorated thin filaments. *J. Mol. Biol.* 50:279–295.

Mozo, A. V., and B. R. Ware. 1984. *J. Biol. Chem.* In press.

Oosawa, F. 1970. Size distribution of protein polymers. *J. Theor. Biol.* 27:69–86.

Oosawa, F., and M. Kasai. 1971. Actin. *In* Biological Macromolecules. Timasheff and Fasman, Editors., Marcel Dekker, Inc., New York. 5:261–322.

Pardee, J. D., and J. A. Spudich. 1982. Mechanism of K^+-induced actin assembly. *J. Cell Biol.* 93:648–654.

Peters, R., J. Peters, K. H. Tews, and W. Bahr. 1974. A microfluorimetric study of diffusion in erythrocyte membranes. *Biochim. Biophys. Acta.* 367:282–294.

Rees, M. K., and M. Young. 1967. Studies on the isolation and molecular properties of homogeneous globular actin. *J. Biol. Chem.* 242:4449–4458.

Rouayrenc, J.-F., and F. Travers. 1981. The first step in the polymerization of actin. *Eur. J. Biochem.* 116:73–77.

Schurr, J. M. 1980. A theory of electrolyte friction on translating polyelectrolytes. *Chem. Phys.* 45:119–132.

Spudich, J. A., and S. Watt. 1971. The regulation of rabbit skeletal muscle contraction. *J. Biol. Chem.* 246:4866–4871.

Straub, F. B., and G. Feuer. 1950. Adenosinetriphosphate the functional group of actin. *Biochim. Biophys. Acta.* 4:455–470.

Tait, J. F., and C. Frieden. 1982. Polymerization and gelation of actin studied by fluorescence photobleaching recovery. *Biochemistry.* 21:3666–3674.

Tanford, C. 1961. Physical Chemistry of Macromolecules. J. Wiley & Sons, Inc., New York. 394.

Taylor, D. L., and Y.-L. Wang. 1978. Molecular cytochemistry: incorporation of fluorescently labeled actin into living cells. *Proc. Natl. Acad. Sci. USA.* 75:857–861.

Taylor, D. L., J. Reidler, J. A. Spudich, and L. Stryer. 1981. Detection of actin assembly by fluorescence energy transfer. *J. Cell Biol.* 89:362–367.

Tellam, R., and C. Frieden. 1982. Cytochalasin D and platelet gelsolin accelerate actin polymer formation. A model for regulation of the extent of actin polymer formation in vivo. *Biochemistry*. 21:3207–3214.

Wang, Y.-L., and D. L. Taylor. 1980. Preparation and characterization of a new molecular cytochemical probe: 5-iodoacetamidofluorescein-labeled actin. *J. Histochem. Cytochem.* 28:1198–1206.

Wang, Y.-L., and D. L. Taylor. 1981. Probing the dynamic equilibrium of actin polymerization by fluorescence energy transfer. *Cell.* 27:429–436.

Wang, Y.-L., F. Lanni, P. L. McNeil, B. R. Ware, and D. L. Taylor. 1982. Mobility of cytoplasmic and membrane-associated actin in living cells. *Proc. Natl. Acad. Sci. USA.* 79:4660–4664.

Wegner, A. 1976. Head to tail polymerization of actin. *J. Mol. Biol.* 108:139–150.

Wegner, A. 1982. Spontaneous fragmentation of actin filaments in physiological conditions. *Nature (Lond.).* 296:266–267.

Wegner, A.. and P. Savko. 1982. Fragmentation of actin filaments. *Biochemistry*. 21:1909–1913.

Wojciesczyn, J. W., R. A. Schlegel, E.-S. Wu, and K. A. Jacobson. 1981. Diffusion of injected macromolecules within the cytoplasm of living cells. *Proc. Natl. Acad. Sci. USA.* 78:4407–4410.

Yin, H. L., J. H. Hartwig, K. Maruyama, and T. P. Stossel. 1981. Ca^{+2} Control of Actin Filament Length. *J. Biol. Chem.* 256:9693–9697.